Journal of Marine Science and Technology, Vol. 26, No. 2, pp. 217-227 (2018)
DOI: 10.6119/JMST.2018.04_(2).0009

THE INVESTIGATION OF THE TWO-PHASE THERMOSYPHON PERFORMANCE LIMIT

Chih-Chung Chang[1], Zun-Long Huang[2], Yuan-Ching Chiang[3], and Sih-Li Chen[2]

Key words: thermosyphon, boiling limit, entrainment limit, thermal resistance.

ABSTRACT

In a steel plant, waste heat recovery systems of hot-blast furnace are characterized by high-temperature exhaust gas from a hot stove that flows through heat pipe heat exchangers. By heating gas in a hot stove and combustion air in a blast furnace, stable and balanced heat exchange efficiency is achieved in this system. The thermosyphon, which is also known as a gravitational heat pipe, uses latent heat to transfer the heat. In this article, heat pipe performance limits, including entrainment and boiling limits, are experimentally and theoretically investigated. Heat pipe tube lengths of 130 mm, 200 mm, and 300 mm were used in the experiment, and the operating temperature and heat transfer rates obtained were compared in a MATLAB prediction program to determine when boiling and entrainment limits occur. The precision comparisons of the theoretical and experimental results were 8.7% and 6.7%, respectively. Therefore, a standard test method and prediction program for boiling and entrainment limits are presented in this study, and the heat transfer phenomena in heat pipes of any scale are explained when these limits occur. Additionally, according to data from the China Steel Corporation, the capacity limit of the heat transfer rate for the heat pipe in this study is calculated at 8,370 W.

I. INTRODUCTION

Waste heat recovery systems are designed for heat pipe heat exchangers in steel plants. The characteristics of these heat recovery systems include original high-temperature exhaust gas from a hot stove flowing through heat pipe heat exchangers. Heated gas from a hot stove and blast furnace and combustion air are shown in Fig. 1. With long-term use, the performance of this system will be attenuated, so it must be updated. In the past, research and development often took place through experimental performance testing, but the heat pipes used in waste heat recovery systems are too large for this. Tests that use a large single tube are essentially difficult, so the development of a performance prediction program to understand the performance limits of heat pipes can reduce costs by limiting the number of times experimental tests need to be conducted.

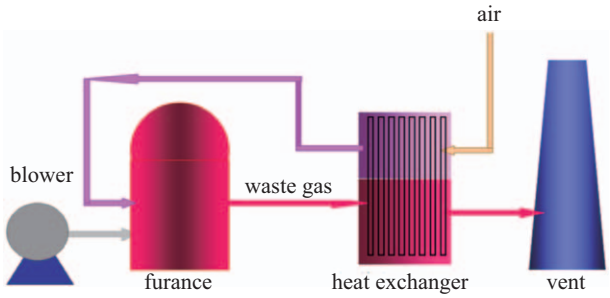

Fig. 1. Blast furnace waste heat recovery systems.

The principle of heat pipe heat exchange is the application of physical phenomena of water vapor condensation to the two-phase heat transfer. When the water inside the tube absorbs heat, it changes from liquid to gas form, and steam moves along the heat pipe to the cooling side and then condenses. Heat that was previously absorbed through vaporization is released into blast furnace gas or combustion air, completing a thermal cycle and continuing to repeat this heat exchange. The heat pipe operating temperature is maintained at the heat absorption of the equilibrium temperature. In order to maximize the efficiency of a heat pipe heat exchanger, some heat pipes are coupled with the outer ring of large radial fins to increase the heat transfer area, and more heat pipes are added to the heat exchanger in a fixed space.

Kutateladze (1972) used dynamic stability criteria to define a Kutateladze number. Asselman and Green (1973) found far less thermal resistance at the liquid-gas interface and in the vapor flow in the adiabatic section than elsewhere. The entrainment limit coincides with a temperature shock phenomenon on the wall of the evaporator. When the evaporator temperature rises suddenly, the boiling limit can be determined (Chen, 1983). Faghri et al. (1989) determined that a large diameter of a non-core heat

Paper submitted 02/10/17; revised 07/27/17; accepted 01/24/18. Author for correspondence: Sih-Li Chen (e-mail address: slchen01@ntu.edu.tw).
[1] *China Steel Corporation, 1, Chung Kang Rd., Hsiao Kang, Kaohsiung, Taiwan, R.O.C.*
[2] *Department of Mechanical Engineering, National Taiwan University, Taipei, Taiwan, R.O.C.*
[3] *Department of Mechanical Engineering, Chinese Culture University, Taipei, Taiwan, R.O.C.*

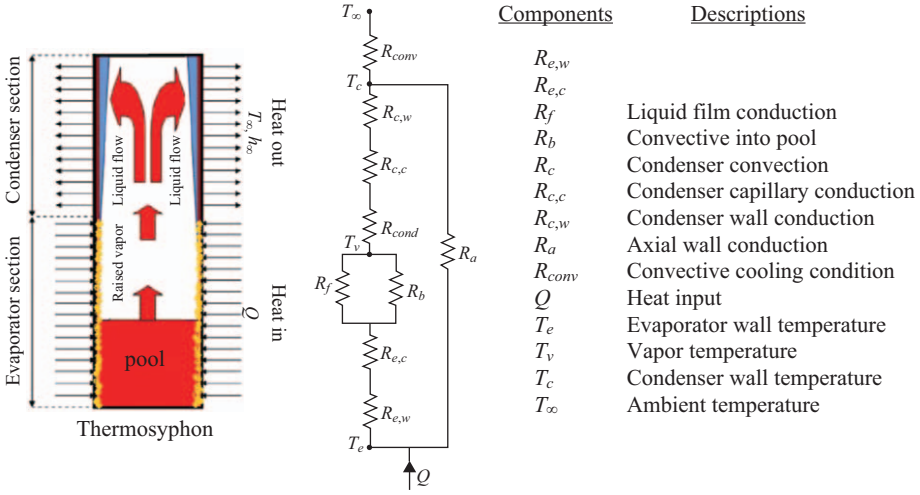

Fig. 2. Thermal resistance model.

pipe at a relatively high heat flux will cause overflow oscillation (i.e., flooding oscillation), leading to an overflow limit for heat transfer. A related study showed that the boiling limit occurs in the nucleate boiling stage (Chi, 1976); the Clausius-Clapeyron equation in a bubble liquid equilibrium describes the relationship between system pressure and temperature. Nguyen and Groll (1981) investigated the entrainment or flooding limit of a copper-water thermosyphon (which had fine circumferential grooves on its inner surface), including small inclination angles of 1°, 2°, and 5° in a horizontal direction. As the heat load increased, the surface temperature profile of the thermosyphon was recorded. Temperature fluctuations occurred and were accompanied by a periodic noise at a particular power level. Thermosyphon operation is limited by dry-out if the filling ratio is below the optimum value, while entrainment or flooding prevails if the filling ratio exceeds the optimum value (Bezrodny et al., 1994).

This study aims to develop and apply programs to predict the performance limits of different sizes of heat pipe, and also to estimate the amount of heat transfer at different operation temperatures. In addition to the heat pipe thermal resistance model presented, this research is essential for establishing experimental performance testing of heat pipes in terms of total thermal resistance, which includes that of the wall and that between the capillary structure and working fluid. The accuracy of the prediction program was tested through a comparison with the study experiments; the average errors for the thermal resistance of the evaporator and condenser were within 10%.

II. RESEARCH METHOD

The purpose of this study is to establish simulation and calculation software that can quickly calculate the heat transfer limits for heat pipes of different sizes and in operating environments. The software can also calculate thermal resistance and vapor temperature inside the heat pipe.

1. Thermal Resistance Model

In this experimental system, the total thermal resistance includes the evaporator section of the wall thermal resistance $R_{e,w}$, the evaporator section of capillary thermal resistance $R_{e,c}$, the evaporator section of thin-film thermal resistance R_{film}, the condenser section of condensation thermal resistance R_{cond}, the condenser section of capillary thermal resistance $R_{c,c}$ the condenser section of the wall thermal resistance $R_{c,w}$ the condenser section of convective thermal resistance R_{conv} and fin thermal resistance R_{fin} in Fig. 2. In this study, the axial wall conduction is not considered for the experimental data and the predicted data. The impacts of wall conduction on the supplied heater power Q are radius direction instead of axial direction. The contact thermal resistance is neglected in this study because the order of contact thermal resistance is smaller than other thermal resistance (ISO, 1995). The formula of the total thermal resistance is as following.

$$R_{total} = R_{e,w} + R_{e,c} + \frac{R_b R_{film}}{R_b + R_{film}} + R_{cond} + R_{c,c} + R_{c,w} + R_{conv} + R_{fin} \quad (1)$$

The definition of each thermal resistance is as following.

The wall evaporator thermal resistance is defined as follows:

$$R_{e,w} = \frac{\ln\left(\frac{d_o}{d_i}\right)}{2\pi L_e K_p} \quad (2)$$

The capillary evaporator thermal resistance is defined as follows:

$$R_{e,c} = \frac{\ln\left(\frac{d_{o,wick}}{d_{i,wick}}\right)}{2\pi L_e K_{wick}} \quad (3)$$

The boiling evaporator thermal resistance is defined as follows (Asselman and Green, 1973):

$$R_b = C_{SF}\frac{h_{lv}Pr_l}{qCp_l}\left\{\frac{q/A_{die}}{\mu_l h_{lv}}\sqrt{\frac{\sigma}{g(\rho_l-\rho_v)}}\right\}^{0.33},\ C_{SF}=0.0202 \quad (4)$$

The thin film evaporator thermal resistance is defined as follows (Asselman and Green, 1973):

$$R_{film} = C_{SF}\frac{3}{4A_e}\left\{\frac{\rho_l^2 k_l^3 g h_{fg}}{4\mu_l\left(T_{w,e}-T_{w,c}\right)L_e}\right\}^{-0.25} \quad (5)$$

The condensing condenser thermal resistance is defined as follows (Asselman and Green, 1973):

$$\begin{aligned} R_{cond} &= \frac{1}{FA_{cond}}\left\{\frac{\rho_l(\rho_l-\rho_v)k_l^3 g h_{lv}}{\mu_l\left(T_{evap}-T_{cw,m}\right)L_c}\right\}^{-0.25} \\ &= \frac{1}{0.0009Re_v^{0.7643}A_{cond}}\left\{\frac{\rho_l(\rho_l-\rho_v)k_l^3 g h_{lv}}{\mu_l\left(T_{evap}-T_{cw,m}\right)L_c}\right\}^{-0.25} \end{aligned} \quad (6)$$

The capillary condenser thermal resistance is defined as follows:

$$R_{c,c} = \frac{\ln\left(\frac{d_{o,wick}}{d_{i,wick}}\right)}{2\pi L_c K_{wick}} \quad (7)$$

The wall condenser thermal resistance is defined as follows:

$$R_{c,w} = \frac{\ln\left(\frac{d_o}{d_i}\right)}{2\pi L_c K_p} \quad (8)$$

The convection thermal resistance is defined as follows:

$$R_{conv} = \frac{1}{h_{conv}A_{cond}} \quad (9)$$

$$h_{conv} = F\frac{\rho_l(\rho_l-\rho_v)g h_{lv}k_l^3}{\mu_l\left(T_{sat}-T_w\right)d_i} \quad (10)$$

The fin thermal resistance is defined as follows:

$$R_{fin} = \frac{1}{\eta_f A_t h} \quad (11)$$

The fin efficiency is defined as follows:

$$R_{fin} = \frac{1}{\eta_f A_t h} \quad (12)$$

$$\eta_0 = 1-\frac{A_f}{A_o}(1-\eta) \quad (13)$$

$$A_o = A_f + A_b \quad (14)$$

where A_o is the total air-side surface area of heat exchanger, A_f is the surface area of fin and A_b is the surface area of bare tube.

The convective heat transfer coefficient is defined as follows:

$$h = \left(\frac{K_w}{d_i}\right)\frac{\left(Re_{Dw}-1000\right)Pr_w\left(\frac{f_i}{2}\right)}{1+12.7\sqrt{\frac{f_i}{2}}\left(Pr_i^{\frac{2}{3}}-1\right)} \quad (15)$$

$$f_i = \left[1.58\ln\left(Re_{Dw}\right)-\right]3.28^{-2} \quad (16)$$

where Re_{Dw} is the tube-side Reynolds number, P_{rw} is the Prandtl number of water flowing inside tube and k_w is the thermal conductivity of water.

The heat pipe total thermal resistance is defined as follows:

$$R_{p,total} = \frac{T_e-T_c}{Q} = R_{e,w}+R_{e,c}+\frac{R_b R_f}{R_b+R_f}+R_{cond}+R_{c,c}+R_{c,w} \quad (17)$$

The system total thermal resistance is defined as follows:

$$\begin{aligned} R_{s,total} = \frac{T_e-T_\infty}{Q} &= R_{e,w}+R_{e,c}+\frac{R_b R_f}{R_b+R_f}+R_{cond} \\ &\quad +R_{c,c}+R_{c,w}+R_{conv}+R_{fin} \end{aligned} \quad (18)$$

2. Heat Pipe Limits

1) Entrainment Limit

In the heat transfer process, vapor and liquid flow in opposite directions in the heat pipe and come into contact with each other. The condensation film flows down to the reflux, while rising vapor generates shear stress at the interface. As a result, the liquid film undergoes fluctuations, or droplet dispersal, which cause the entrainment limit. The rising steam completely prevents the condensation liquid from flowing down, and the evaporator dries out. Thus, the heat pipe performance reaches its limit. When the entrainment phenomenon occurs, transient temperature and pressure oscillation values can be observed. Faghri et al. (1989) proposed an empirical formula for the entrainment limit:

Table 1. The effective heat transfer coefficient for different capillary structure.

Wick structures	k_{eff}
Wick and liquid in series	$\frac{k_l k_w}{\varepsilon k_w + k_l(1-\varepsilon)}$
Wick and liquid in parallel	$\varepsilon k_w + k_w(1-\varepsilon)$
Wrapped screen	$\frac{k_l\left[(k_l+k_w)-(1-\varepsilon)(k_l-k_w)\right]}{(k_l+k_w)(k_l-k_w)(1-\varepsilon)}$
Packed spheres	$\frac{k_l\left[(2k_l+k_w)-2(1-\varepsilon)(k_l-k_w)\right]}{(2k_l+k_w)(k_l-k_w)(1-\varepsilon)}$
Rectangular grooves	$\frac{\omega_l k_l + k_w\delta + \omega_l k_l(0.185\omega_l k_w + \delta k_l)}{(\omega+\omega_f)(0.185\omega_f k_l + \delta k_l)}$

Table 2. The dimension of heat pipe.

	Dimension (mm)		
Total length	130	200	300
Evaporation length	65	100	150
Condensation length	65	100	150
Outer diameter	7		
Inner diameter	5		
Heating length	55	70	108
Fill Ratio	18%		
Groove dimensions	$W = 0.204$, $W_f = 0.126$, $\delta = 0.204$		
Sintered thickness	$t = 0.41$		

$$q_{ent} = 2\tanh^2(0.5Bo^{0.25})A_v h_{lv}((\rho_l^{-0.25}+\rho_v^{-0.25})^{-2}(g\sigma(\rho_l-\rho_v))^{0.25}) \quad (19)$$

where h_{lv} is evaporation enthalpy and Bo is boiling number.

As seen in Eq. (19), the entrainment limit is independent of the length of the heat pipe, but it is related to the thermodynamic properties of water and the heat pipe diameter.

2) Boiling Limit

In this study, the capillary structure in the evaporator enhances the boiling mechanism of the heat pipe. The heat flux in the heating process gradually increases the boiling point to a peak, until even the wall surface of the evaporator is covered with steam bubbles. Finally, an extreme wall temperature causes the evaporator to reach the burnout point. The boiling limit is caused by nucleate boiling, bubble growth, and the consolidation of complex physical phenomena. Nucleation occurs in the gas core in the liquid, which generates bubbles. As mentioned above, Chi (1976) uses the Clausius-Clapeyron equation to express a bubble liquid equilibrium. The relationship between system pressure and temperature is dynamic. Bubbles will grow in the capillary structure and hinder the backflow of liquid, resulting in the boiling limit. Eq. (20) is the theoretical formula of the boiling limit. From Eq. (20), the boiling limit is affected by the length of the heat pipe evaporator, and is related to the capillary structure; keff is calculated in Table 1.

$$q_{boil} = \frac{2\pi L_e k_{eff} T_v}{h_{fg}\rho_v \ln\left(\frac{r_i}{r_v}\right)}\left(\frac{2\sigma}{r_n} - P_c\right) \quad (20)$$

where r_n is nucleation site radius.

3. Experiment Setup

This experiment was performed with three different heat pipes, with total lengths of 130 mm, 200 mm, and 300 mm, respectively (Table 2). Each pipe had a diameter of 7 mm and a fill ratio of 18%. After preliminary degassing, a pump was used to remove the air from each heat pipe, thereby reducing the system pressure to 0.021 MPa. The fluid used for the experiment was water. The heating power plateaued at 50 W, and the operating temperature range for the experiment was 400-500 K. The maximum temperature detected was 500 K. The groove and sintering of the composite structure constituted the tube structure; the groove collected the condensed water. The experimental sys-

Table 3. The manufacturers, models and accuracies of the instruments.

Instruments	Accuracy and model
Thermocouple	±0.5°C, T type
Recorder	YOKOGAWA
Power supply	±(0.4%)
Fan	Fan speed error 2%

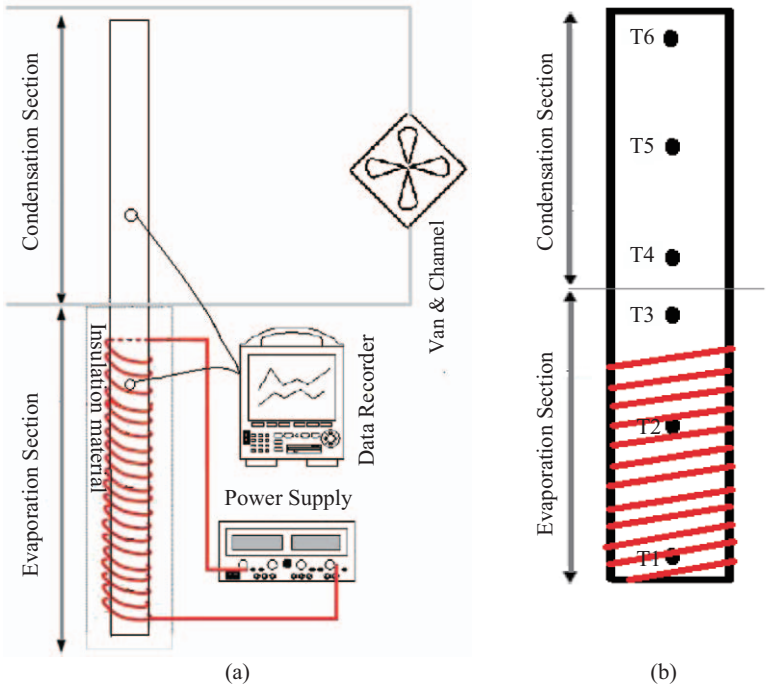

Fig. 3. (a) Experimental system diagram. (b) Measured temperature points location.

tem is illustrated in Fig. 3(a). To observe the limits of the heat pipe's wall temperature, constant wind speed was applied to the condenser section. The different segments of the pipe were subjected to different wind speeds to test their heat transfer limits. The evaporator was heated by an electrical system and the condenser section was placed inside the duct to allow the cooling fan to remove the heat. Table 3 details the manufacturers, models, and accuracy specifics for the instruments used in this experiment. The heat pipe wall temperature was measured in six different locations; Fig. 3(b) shows the relative position of each measurement point. The start-up performance was investigated and the measurements were taken at the steady states. The steady state is ascertained from the effective thermal resistance R_{eff}, which is determined by averaging thermal resistance before dry-out occurs; the maximum heating power $Q_{\max}$ is found at the dry-out point. The effective thermal resistance of the heat pipe is calculated as

$$R_{eff} = \frac{T_e - T_c}{Q} \tag{21}$$

where T_e and T_c are the average temperatures of the evaporation section and the condensation section, respectively, and Q is the corresponding heating power. The manufacturers, models, and accuracies of the instruments are addressed in Table 3. Based on the uncertainty analysis proposed by ISO standards (ISO, 1995), the uncertainties of temperature and thermal resistance measurement are ±0.5% and ±5%, respectively. The heat loss measured in this system was within 5% of the overall heat. Therefore, heat loss was neglected in this study.

III. RESULTS AND DISCUSSION

1. The Experimental Results of the Performance Limits

While constant wind speed was applied to the condenser section, the steam temperature and heat transfer increased, finally reaching an operating limit. To determine the heat pipe's limits, Chi (1976) proposed the temperature phenomena to set the criteria. The entrainment limit occurs when the evaporator wall temperature oscillates. The boiling limit occurs when the evaporator wall temperature rises suddenly. Figs. 4(a) and (b) show the average temperature of all recorded data, which were synchronously recorded. Fig. 4(a) indicates that, when no wind was applied to the 200 mm heat pipe, a sudden temperature increase

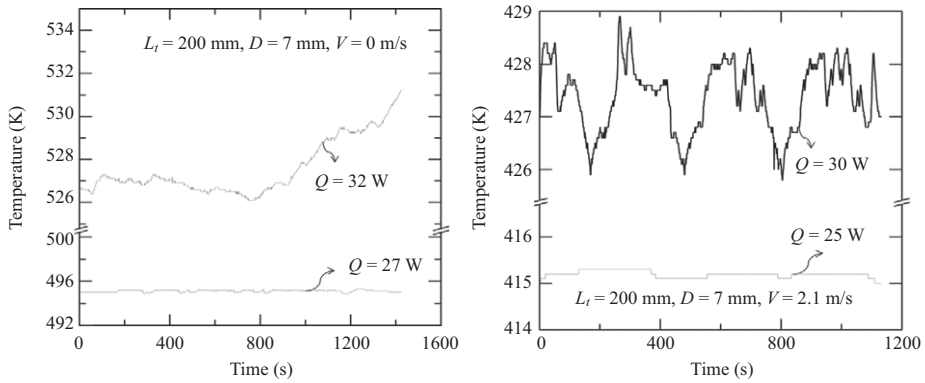

Fig. 4. (a) The temperature distribution of the 200 mm heat pipe at velocity of 0 m/s. (b) The temperature distribution of the 200 mm heat pipe at velocity of 2.1 m/s.

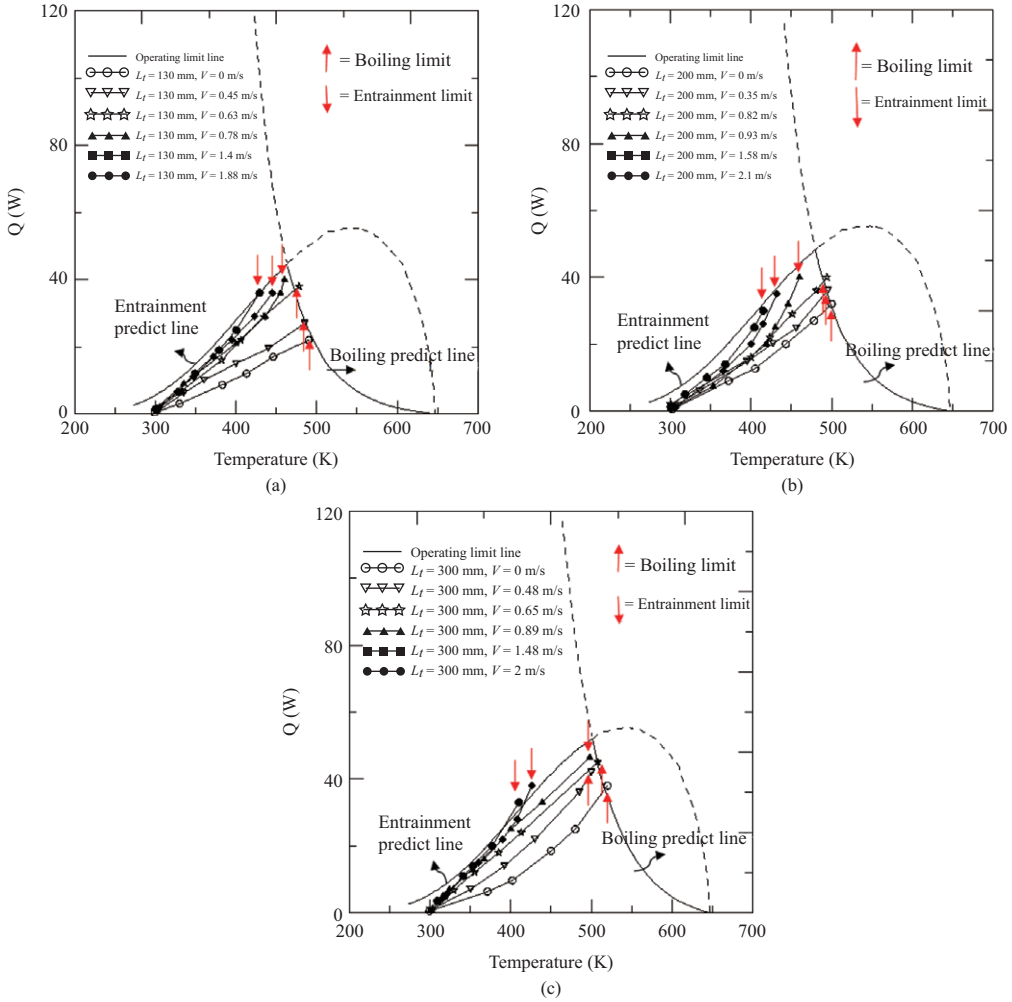

Fig. 5. (a) The comparison of experimental and theoretical results of the130 mm heat pipe. (b) The comparison of experimental and theoretical results of the 200 mm heat pipe. (c) The comparison of experimental and theoretical results of the 300 mm heat pipe.

caused the boiling limit. Fig. 4(b) shows that, for a speed of 2.1 m/s, the entrainment limit occurred when the temperature oscillated. This study used these findings as the reference point during other experiments. Nguyen and Groll (1981) found that particular power temperature fluctuations occurred at the entrainment or flooding limit of copper-water thermosyphons.

Fig. 5(a) shows the 130 mm heat pipe with wind speeds of 0 m/s, 0.45 m/s, 0.63 m/s, 0.78 m/s, 1.4 m/s, and 1.88 m/s. The

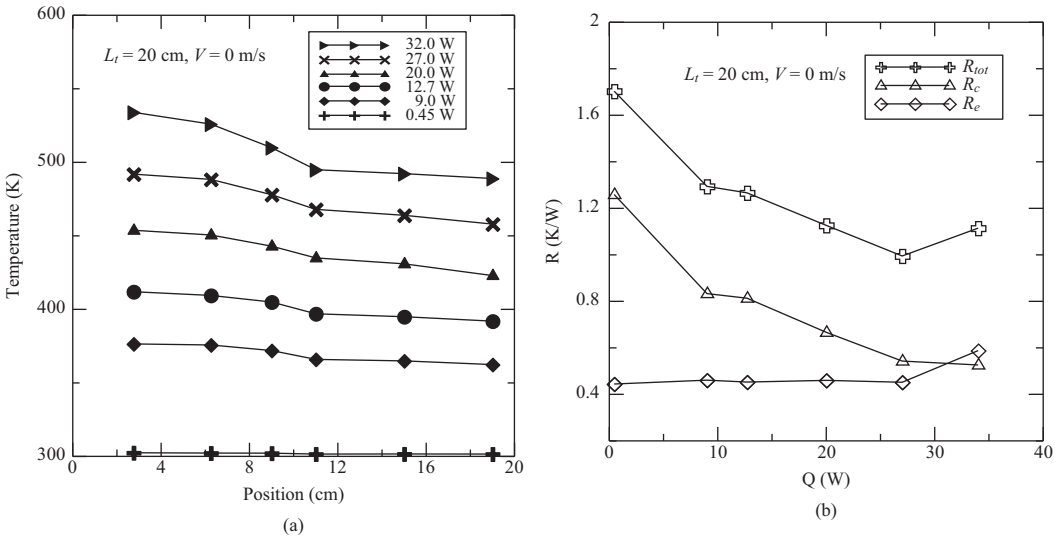

Fig. 6. (a) The temperature distribution of the 200 mm heat pipe at different positions with 0 m/s velocity. (b) The thermal resistance distribution of the 200 mm heat pipe at 0 m/s velocity for different heating power.

operating temperature (T_v) changed with an increase in heating power until it reached the limit of the phenomenon. Using the same heat flux, when the wind speed increased, the vapor temperature decreased. This indicates that the capacity of the condenser increases as the wind speed increases; the wind quickly removes the heat from the heat pipe. At a lower heating power of less than 5 W, the impact of the wind speed on the vapor temperature was small. The two-phase heat transfer mechanism was not initiated in this instance, and heat transference was dependent on the wall. When the heating power was set anywhere from 10 W to 30 W, the wind speed influenced the performance of the heat pipe's cooling capacity. There was a temperature difference of about 70 K between wind speeds of 0 m/s and 1.88 m/s when the heating power was set at 20 W. A comparison of experimental values with theoretical values shows that the heat transfer reached the limits more quickly when the wind speed was 0-0.63 m/s. When the wind speed increased (0.78-1.88 m/s) with a corresponding rise in heating power, the evaporator wall temperature experienced the oscillation phenomenon. This was due to the large amount of steam affecting the return liquid, which caused a shock in the wall temperature.

Fig. 5(b) shows a 200 mm heat pipe with wind speeds of 0 m/s, 0.35 m/s, 0.62 m/s, 0.93 m/s, 1.58 m/s, and 2.1 m/s, in which the vapor temperature changed with the increase of the heat flux. Experimental and theoretical results of entrainment and boiling limit lines can be drawn together. The arrow points indicate the experimental limit value when the entrainment or boiling limit occurred. As shown in Fig. 5(b), when the heating power was increased, the vapor temperature rose. The experimental result trends were roughly the same as those of the 130 mm heat pipe. The theoretical formula also shows that the entrainment limit was not absolutely dependent on the size and length of the heat pipe. The boiling limit, however, increased as the heat pipe lengthened.

Fig. 5(c) shows a 300 mm heat pipe with wind speeds of 0 m/s, 0.48 m/s, 0.65 m/s, 0.89 m/s, 1.48 m/s, and 2 m/s. The figure shows that the vapor temperature changed with an increase of the heat flux. Fig. 5(c) presents the theoretical entrainment limit and boiling limit. The arrow points indicate the experimental values at which the entrainment or boiling limit occurred. The experimental values were consistent with the trends seen in the 130 mm and 200 mm heat pipes. As before, the vapor temperature rose to match an increase in the heating power; as the wind speed grew, the vapor temperature decreased. Due to an increase in the condenser capacity, the heat quickly exited the heat pipe. At a wind speed of 0.89 m/s and a heating power of 46.5 W, the vapor temperature reached 498 K, which is closer to the theoretical value of the boiling limit. The wall temperature of the evaporator also experienced oscillation (entrainment limit).

2. Thermal Resistance Analysis

To better understand the heat transfer phenomena of the entrainment and boiling limits of the heat pipe, the 200 mm heat pipe was subjected to temperature changes to obtain experimental results of R_e, R_c and R_t. Fig. 6(a) shows the locations along the heat pipe of the six wall temperature data points, located from 0 cm to 20 cm, which are designated T1 to T6 in Fig. 3(b). The temperature of the 200 mm heat pipe, with a wind speed of 0 m/s, increased with the increase of the heating power. At 0.45 W, the heat pipe temperature difference was very small. Fig. 6(b) presents the total thermal resistance of the heat pipe (1.7 K/W), the evaporator thermal resistance (0.4 K/W), and the condenser thermal resistance (1.3 K/W). With an increase in heating power, the condenser thermal resistance and total thermal resistance decreased. When the heating power was 27 W, the total thermal resistance was 0.99 K/W, the evaporator thermal resistance was 0.45 K/W, and the condenser

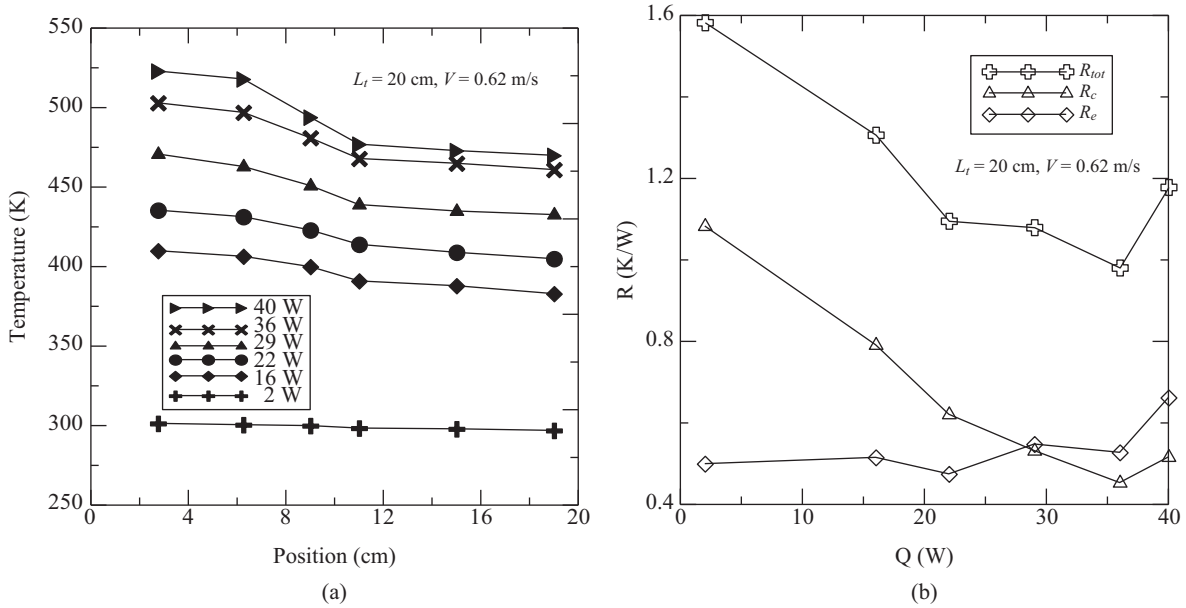

Fig. 7. (a) The temperature distribution of the 200 mm heat pipe at different positions with 0.62 m/s velocity. (b) The thermal resistance distribution of the 200 mm heat pipe at 0.62 m/s velocity with different heating power.

thermal resistance was 0.54 K/W. The condenser thermal resistance remained greater than the evaporator thermal resistance. Both the condenser and the evaporator thermal resistance changed before the heat transfer limits occurred. At a heating power of 32 W, the evaporator thermal resistance rose from 0.45 K/W to 0.59 K/W, and the total thermal resistance increased to 1.1 K/W; the condenser thermal resistance, however, dropped to 0.52 K/W. The temperature of the evaporator also increased, and the wall bubbles that were generated formed a thin film. The heat pipe subsequently reached the boiling limit.

Fig. 7(a) shows the temperature distribution for a 200 mm heat pipe with a wind speed of 0.62 m/s and increasing heating power. Fig. 7(b) indicates the change of the total thermal resistance, the evaporator thermal resistance, and the condenser thermal resistance with increasing heating power. At 2 W, the heat pipe temperature was about 300 K, and the average temperature difference of the evaporator and condenser was about 3 K. The condenser thermal resistance was 1 K/W at a wind speed of 0.35 m/s and a heating power set at 1.6 W. The condenser thermal resistance was 0.9 K/W at a wind speed between 0.35 m/s and 0.62 m/s. The heat transfer process did not initiate. Heating power continued to increase with a decrease in the total thermal resistance and condenser thermal resistance. At a heating power of 29 W, the evaporator thermal resistance was 0.55 K/W, and the condenser thermal resistance was 0.53 K/W. The heat of the condenser was constantly removed by way of forced convection. The condenser thermal resistance was less than the evaporator thermal resistance. As heating power continued to increase, the total thermal resistance decreased. At 40 W, the total thermal resistance jumped to 1.2 K/W, the evaporator thermal resistance increased to 0.66 K/W, and the condenser thermal resistance reached 0.51 K/W. The wall temperature of the evaporator experienced short oscillations before the phenomenon increased. This meant that the boiling limit was reached. The thermal resistance ranges of the evaporator and condenser were 0.5-0.65 K/W and 0.42-1.1 K/W. The thermal resistance values observed were generally higher than those found in previous studies. Takurou and Nagai (2015) found that a higher ratio of non-condensable gas (NCG) would increase the thermal resistance. Thus, it appears that a NCG was present in the heat pipe tested.

Fig. 8(a) shows the temperature distribution for the total length of a 200 mm heat pipe at a wind speed of 0.93 m/s and increasing heating power. Fig. 8(b) indicates the total thermal resistance, evaporator thermal resistance, and condenser thermal resistance with increasing heating power. At a low heating power of 0.7 W, the heat pipe temperature was low, and the total thermal resistance was very high (approximately 1.6 K/W). The evaporator thermal resistance and condenser thermal resistance were 0.5 K/W and 1.1 K/W, respectively. When the heating power increased to 7 W, the condenser thermal resistance dropped to 0.47 K/W. This is indicative of good heat pipe condenser cooling capacity. The heat will be quickly and effectively removed, allowing the steam to condense quickly. When the heating power was 40 W, the wall temperature began to oscillate. This was caused by the evaporation of the upper membrane, releasing a large amount of steam. Liquid film began to accumulate at the top of the condenser section, while this section also had a larger reflow resistance. The condenser temperature gradient made the wall temperature uneven, resulting in the entrainment limit. The backflow of the liquid film in the tube caused large amounts of shear stress drag, in turn causing the condensing section of the liquid film to thicken. The condenser thermal resistance was high. At this time, there was no liquid film in the evaporator. The evaporator thermal resistance was

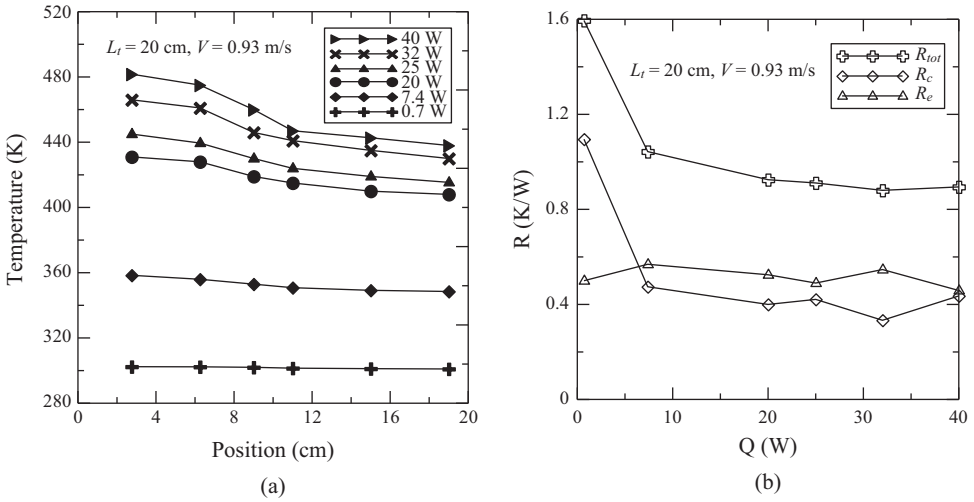

Fig. 8. (a) The temperature distribution for the length of 200 mm heat pipe at different positions with wind speed 0.93 m/s. (b) The distribution of thermal resistance with the changes of heating power for the length of 200 mm heat pipe at wind speed 0.93 m/s.

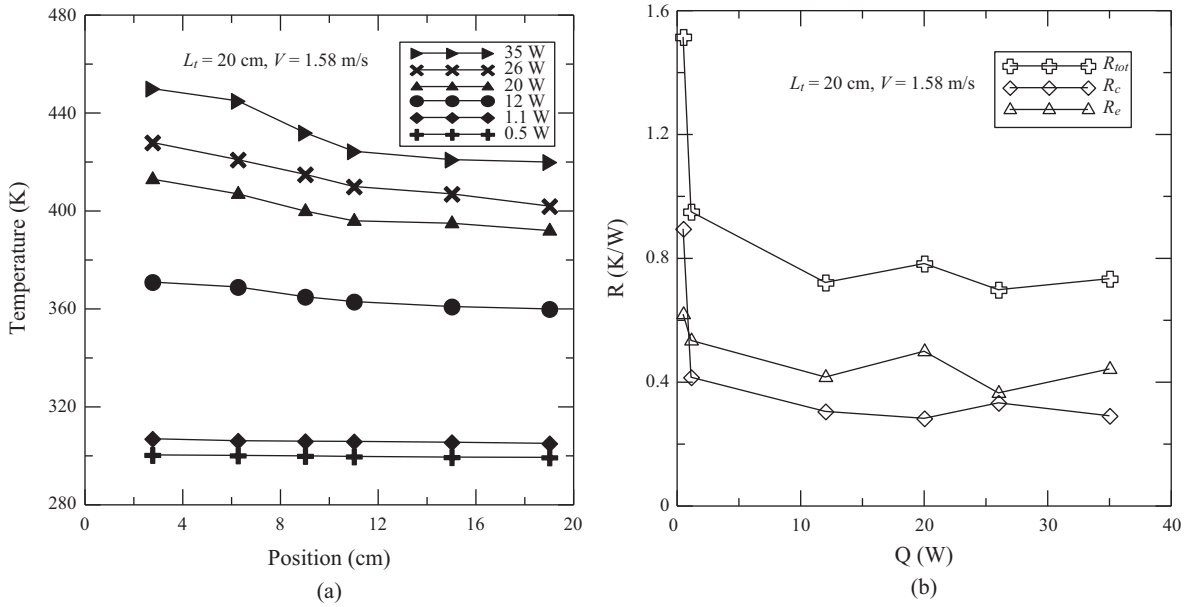

Fig. 9. (a) The temperature distribution for the length of 200 mm heat pipe at different positions with wind speed 1.58 m/s. (b) The distribution of thermal resistance with the changes of heating power for the length of 200 mm heat pipe at wind speed 1.58 m/s.

small. When the liquid vapor shear stress could not push the liquid film up, the liquid film dropped. This caused the evaporator thermal resistance to grow and the condenser thermal resistance to decrease, as shown in Fig. 9(b). The thermal resistance during the entrainment limit constituted the shock leading to the change in behavior.

Fig. 9(a) shows that the heat pipe temperature increased when the heating power was placed along the total length of the 200 mm pipe, and a wind speed of 1.58 m/s was applied. Fig. 9(b) shows that the total thermal resistance, evaporator thermal resistance, and condenser thermal resistance changed with an increase of the heating power and a wind speed of 1.58 m/s. With a heating power of 0.5 W, the heat pipe did not function. The total thermal resistance was 1.5 K/W, the evaporator thermal resistance was 0.62 K/W, and the condenser thermal resistance was 0.89 K/W. With the increase of heating power, the thermal resistance gradually decreased. This means that a two-phase heat transfer mechanism began within the heat pipe. At 1.12 W, the total thermal resistance was 0.95 K/W, the evaporator thermal resistance was 0.53 K/W, and the condenser thermal resistance was 0.41 K/W. The condenser thermal resistance was lower than the evaporator thermal resistance. Each temperature point exhibited a rise in temperature with an increase of the heating power. The thermal resistance showed only a slight change from 12 W to 35 W. The total thermal resistance was approximately 0.7 K/W, the evaporator thermal

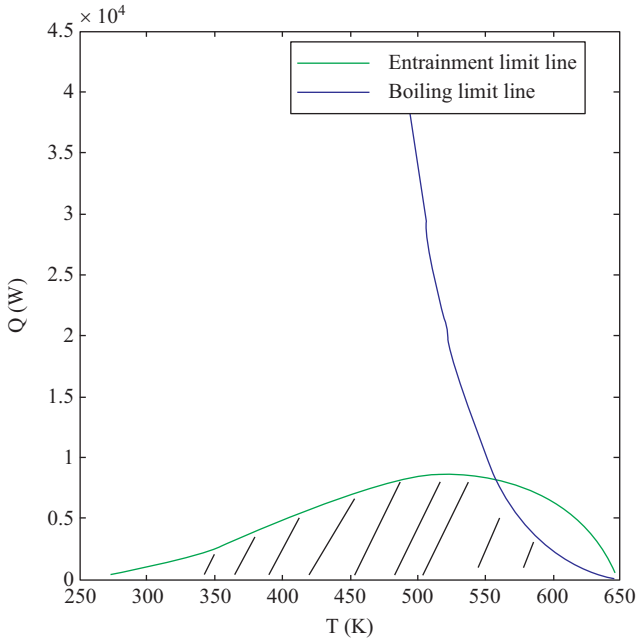

Fig. 10. The effective operating temperature with the relation of heat transfer rate.

resistance was 0.4 K/W, and the condenser thermal resistance was 0.3 K/W. At the entrainment limit, there was no sudden increase or decrease in thermal resistance, but the changes of the heat pipe temperature were observed in the broader slope of the evaporator temperature, as shown in Fig. 9(a).

As shown in Figs. 6-9, the data was temporally averaged. These temporal averages are defined by the average temperature of an evaporator section. The oscillating ranges of the data were around 3-10 K.

Using the prediction program, this study provided the effective operating area between operating temperature and heat transfer rate according to the dimensions of a heat pipe, as shown in Fig. 10. The China Steel Cooperation stated that the operating temperature was around 277°C. For the given dimensions of the heat pipe, the program calculated that the heat transfer rate of the boiling limit was 9,928 W, and the heat transfer rate of the entrainment limit was 8,370 W. This indicates that the capacity limit of heat transfer rate for the heat pipe is 8,370 W.

IV. CONCLUSIONS

This study uses experiments combined with theory to investigate the performance limits of heat pipes. From the experimental results, the cooling capacity of the condenser section has a great influence on the performance of the heat pipe. If the wind speed is low, the thermal resistance will be very high, and performance decreases. When the wind speed increases, the heat of the pipe is quickly and efficiently removed, so that the vapor temperature in the tube is less affected by it. The entrainment limit may be reached with a high amount of heat transfer. A prediction program was used to obtain results for the boiling limit, and these were compared to the experimental results; there was an average difference of 8.7%. The average difference among the entrainment limit results was 6.7%. There was an average difference of less than 10% between experiments and prediction program results regarding the thermal resistance of the evaporator and condenser sections. In addition, according to data from the China Steel Corporation, the capacity limit of the heat transfer rate for the heat pipe used in this study is 8,370 W. The experimental and program data is very similar, indicating that this experimental method is fast and accurate; hence, this prediction program can be used as a test standard for the results of future experiments on the operating limits of other sizes of heat pipe.

V. NOMENCLATURE

A_{die}: Area of the die (m^2)
A_e: Area of evaporator (m^2)
B_o: Boiling number
R_e: Reynolds number
C_{SF}: Coefficient constant
C_{p1}: Specific heat (kJ/kg · K)
D: Diameter (mm)
g: Gravity
h_{lv}: Evaporation enthalpy (kJ)
k: Conductivity (W/m^2 K)
Pr_1: Prandtl number
P_c: $P_c = \frac{2\sigma}{r_c}$, r_c: The effective capillary radius (mm)
q: Heat transfer rate (W)
R_b: The boiling evaporation thermal resistance (K/W)
$R_{e,w}$: The wall evaporation thermal resistance (K/W)
$R_{e,c}$: The capillary evaporation thermal resistance (K/W)
R_{film}: The thin film evaporation thermal resistance (K/W)
R_{cond}: The condensing condensation thermal resistance (K/W)
$R_{c,c}$: The capillary condensation thermal resistance (K/W)
$R_{c,w}$: The wall condensation thermal resistance (K/W)
R_{conv}: The convection thermal resistance (K/W)
R_{fin}: The fin thermal resistance (K/W)
R_{total}: The total thermal resistance (K/W)
r_n: Nucleation site radius (mm)
T: Temperature (K)
W: Width (mm)

Greek symbol

μ_1: Viscosity (m^2/s)
ρ: Density (kg/m^3)
σ: Surface tension (N/m)
η_f: Fin efficiency
ε: Emissivity
ω: Distance (mm)
δ: Distance (mm)

Subscripts

Boil: Boiling

cw: The wall of condenser
ent: Entrainment
m: Mean
n: Nucleate
l: Liquid
w: Water
v: Vapor

VI. REFERENCES

Asselman, G. A. A. and D. B. Green (1973). Heat Pipes. Phillips Technical Review 16, 169-186.

Bezrodny, M. K. and V. M. Podgoretskii (1994). Flooding and heat transfer limits in horizontal and inclined two-phase thermosiphons. Experimental Thermal and Fluid Science Experimental Thermal and Fluid Science 9, 345-55.

Chi, S. W. (1976). heat pipe theory and practice. McGraw-Hill, New York.

Chen, S. J. (1983). Reflux Condensation and Operating Limits of the Two-Phase Closed Thermosyphon. Dissertation thesis, U.C. Berkeley.

Faghri, M., M. Chen and M. Morgan (1989). Heat Transfer Characteristics in Two-Phase Closed Conventional and Concentric Annular Thermosyphons. Transactions of the ASME Journal of Heat Transfer 111, 611-618.

ISO. (1995). Guide to the expression of uncertainty in measurement. International Organization for Standardization. Geneva, Switzerland.

Kutateladze, S. S. (1972). Elements of Hydrodynamics of Gas-Liquid System. Fluid Mechanics-Soviet Research 1, 29-50.

Nguyen, C. H. and M. Groll (1981). Entrainment or flooding limit in a closed two-phase thermosyphon. Journal of Heat Recovery Systems 1, 275-86.

Tien, C. L. and K. S. Chung (1979). Entrainment Limits in Heat Pipes. AIAA Journal 17, 643-646.

Takurou D. and H. Nagai (2015). Operational Characteristics of the Oscillating Heat Pipe with Noncondensable Gas. Journal of Thermophysics and Heat Transfer 29, 563-571.

Wallis G. B. and S. Makkenchery (1974). The Hanging Film Phenomenon in Vertical Annular Two-Phase Flow. J. Fluids Eng. 3, 297-298.